Direct measurement of multiple instability regions via a Fourier filtering method in an optical pattern forming system

M. Pesch,* E. Große Westhoff,† T. Ackemann,‡ and W. Lange§
Institut für Angewandte Physik, Westfälische Wilhelms-Universität Münster, Corrensstrasse 2/4, D-48149 Münster, Federal Republic of Germany‖
(Received 19 February 2003; published 14 July 2003)

We determine the limits of stability of the homogeneous state of a pattern forming optical system in dependency on the wave number by experimental means. The measurement becomes feasible by adopting a scheme based on a Fourier filtering technique. The system under study is a single-mirror feedback arrangement using sodium vapor as the nonlinear medium. The experiment confirms the existence of multiple instability regions of the homogeneous state expected by theory. The measurements do not agree quantitatively with the marginal stability curve determined by a linear stability analysis of an infinitely extended homogeneous system. We study the system numerically and demonstrate that the results of the simulations for the case of a Gaussian beam can be reproduced by a simple modification of the linear stability analysis which accounts for the finite diameter of the input beam. This explains the wave number dependent systematic deviations between the experiment and the linear stability analysis of the infinitely extended system.

DOI: 10.1103/PhysRevE.68.016209 PACS number(s): 89.75.Kd, 47.54.+r, 42.30.Kq, 42.65.Sf

I. INTRODUCTION

An important feature of pattern forming dissipative systems are the threshold values of the stress parameter at which different spatially inhomogeneous modes arise spontaneously from the homogeneous state. The emerging structures are commonly studied in the Fourier space, where extended patterns are represented by only a few well defined modes [1,2]. Typically, at threshold of the pattern forming instability the homogeneous state becomes unstable against Fourier modes with a well defined wave number. Interesting situations arise if the homogeneous state can become unstable versus multiple different instabilities with different critical wave numbers. Such a situation and the resulting complex dynamics were analyzed experimentally and/or theoretically in nonlinear optical systems [3–8], in directional solidification [9], in the Taylor-Dean instability [10] and in the Faraday instability [11–15]. This list presents only some typical examples and is far from being complete.

If a good model of the experimental situation is at hand, the different instabilities and their boundaries can be obtained by a linear stability analysis (LSA) of the homogeneous state. In contrast, an *experimental* determination of the linear stability of the homogeneous state in dependency on the wave number of the perturbation, is difficult in general. Beyond the threshold of pattern formation a structure with a well defined wave number has already formed and no statement on the stability of other wave numbers can be given. We are not aware of previous measurements of the complete set of marginal stability curves in dependency on the wave number, whereas the Busse balloon—i.e., the subrange of wave numbers allowing for stable patterns (e.g., Ref. [16])—can be accessed by a suitable use of boundary effects [17] or initial conditions [18].

In this paper, we will demonstrate a method giving direct experimental access to the instability boundaries in dependency on the wave number. It is based on the selection of an arbitrary wave number by suppressing all other modes with lower threshold. This is achieved by filtering methods in the Fourier space. It turns out that the marginal stability curves in a finite system differ from the ones predicted by a linear stability analysis of the infinitely extended homogeneous state—as it might have been expected beforehand, of course. The differences between the two cases will be analyzed. Again, it will prove to be enlightening as we can check the consequences in a wide range of wave numbers.

In optics, the Fourier space is directly observable and accessible, since the distribution of a light field in the focal plane of a lens is given by the Fourier transform of the light field in front of the lens. Moreover, by introducing a so-called Fourier filter, which is a combination of two lenses and an aperture, it is possible to manipulate the process of pattern formation directly in the Fourier space. This technique has been widely used to control, steer, and analyze the pattern selection in nonlinear optics [19–24]. In this paper, we use a suitably designed filter in order to analyze the linear stability of the unstructured state in an optical pattern forming system.

II. EXPERIMENT

A. Experimental setup

The system under study belongs to the well known class of single-mirror feedback arrangements [25,26]. In this case, it is based on sodium vapor as the nonlinear medium. A scheme of the experimental setup is shown in Fig. 1. The

*Email address: matthias.pesch@uni-muenster.de
†Email address: grosse.westhoff@uni-muenster.de
‡Email address: t.ackemann@uni-muenster.de
§Email address: w.lange@uni-muenster.de
‖URL: http://www.uni-muenster.de/Physik/AP/Lange/Welcome-e.html

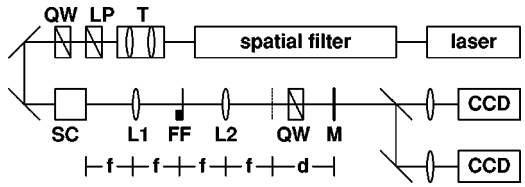

FIG. 1. Scheme of experimental setup. T stands for telescope, LP for linear polarizer, QW for quarter-wave plate, SC for sodium cell, L for lens, FF for Fourier filter, M for mirror, and CCD for charge-coupled device camera.

output of a cw dye laser, which is operating at a frequency some linewidths above the sodium-D_1 line, is being spatially filtered by use of a single-mode fiber. The near-Gaussian output of the fiber is collimated. By means of a 1:1 telescope (T) the beam parameters are adjusted such that the wave front is plane inside the sodium vapor (radius of curvature $R>100$ m, $1/e^2$ radius of the intensity in the beam waist $w_0=1.37$ mm). A circular polarization of light is generated by transmission through a linear polarizer and a quarter-wave plate. The laser beam is injected into a heated cell (SC) containing sodium vapor in a N_2 buffer gas atmosphere. The buffer gas provides a strong homogeneous broadening of the D_1 transition which masks both the hyperfine splitting and the Doppler broadening.

Feedback is provided by the feedback mirror (M, reflectivity $R=99\%$) that is placed at a distance $4f+d$ behind the sodium cell. Due to the quarter-wave plate between the cell and the mirror, the forward and backward beams have opposite helicities. The Fourier filter in the feedback loop consists of two lenses in a $4f$ alignment. In the common focal plane of the lenses, the Fourier transform of the distribution of the field behind the sodium cell can be manipulated by the insertion of a transmission filter. The light transmitted through the feedback mirror is used for detection. The intensity distribution of the transmitted field behind the sodium cell and its optical Fourier transform are imaged onto two charge-coupled device (CCD) cameras.

B. Experimental results

The functionality of the transmission filter used in the experiment is illustrated in Fig. 2. Hexagons, which occur in the system without a filter, are replaced by stripes, which have the same threshold and wave number, if a slit filter is introduced in the Fourier space (cf. also Ref. [23]). Since every component in the Fourier space is also accompanied by its complex conjugate, it is sufficient to use a half-plane filter instead of a slit [Figs. 2(c), 2(g), and 2(k)]. The filter is positioned in order to allow the transmission of the zero-order mode (minimum cutoff frequency $q_{cut}\approx 3.6$ mm^{-1} corresponding to about 2.5 times the $1/e^2$-intensity radius of the input beam at that position) and to achieve a horizontal orientation of the stripe pattern. Wave number selection is realized by a slit filter oriented perpendicular to the edge of the half plane [cf. Fig. 2(d)]. The slit is implemented in the form of two wires of variable width, which can be moved in the vertical direction. The width of the wires has to be carefully chosen in order to select a certain band of wave numbers available for pattern formation, while suppressing the instability of all other wave numbers, which may have a lower threshold, and leaving the zero-order mode unaffected. Having selected a wave number, the threshold can be determined by increasing the laser power until a stripe pattern occurs. Once the pattern has developed, it remains stable if the laser power is increased further.

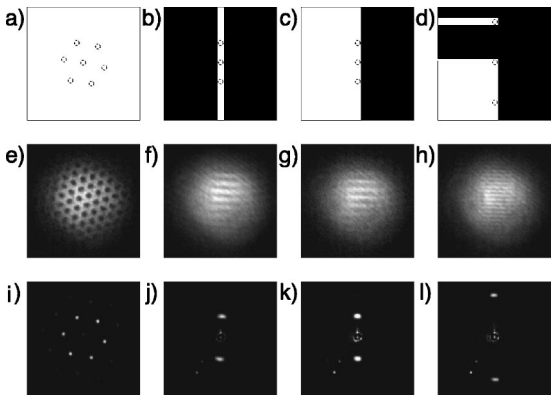

FIG. 2. Sequence of images demonstrating the method used to select stripe patterns with a chosen wave number. Upper row: filtering aperture, black denotes opaque parts and white transparent parts; dashed circles denote the position of the Fourier modes. Middle row: near field intensity distributions. Lower row: far field intensity distributions (zero-order mode suppressed). Parameters: $p_{N_2}=309$ hPa, $T=311.4\,^{\circ}$C, $\Delta=+8$ GHz, $d=77$ mm, (e) $P_0=160$ mW, (f) $P_0=50$ mW, (g) $P_0=45$ mW, (h) $P_0=187$ mW.

The experimentally obtained threshold in dependency on the wave number is depicted in Fig. 3. The result shows three clearly separated regions in which stripes occur. These so-called instability regions are separated by bands of wave numbers where the unstructured state is still observed for the maximum input power available. We interpret the boundaries of the instability regions as the marginal stability curve for the unstructured state. The minima of each curve define the critical wave number and critical pump power for the threshold of each instability region. Within each instability region the shape of the marginal stability curve is approximately parabolic. The threshold for each instability region increases with increasing critical wave number. We will label the in-

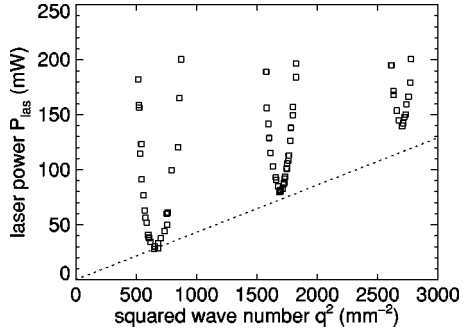

FIG. 3. Experimentally observed instability regions. The dotted line connects the origin with the minimum of the first instability region (see text). Parameters: $T=316.7\,^{\circ}$C, $d=77$ mm, $p_{N_2}=306$ hPa, and $\Delta=5.4$ GHz.

stability regions as regions 1, 2, and 3 starting at low wave numbers.

III. THEORETICAL ANALYSIS

A. Microscopic model

The theoretical analysis for the system under consideration is based on the microscopic model for the interaction of sodium vapor with light (cf. Ref. [27]). The origin of the nonlinearity of the sodium vapor is optical pumping that produces a so-called orientation w, which is proportional to the longitudinal component of the magnetization of the sodium atoms, i.e., of the component in the direction of the laser beam. The properties of the transmitted light are governed by the longitudinally averaged orientation $\phi(x,y) = \int_0^L w(x,y,z)dz$ [28], which determines the complex susceptibility

$$\chi_{\pm} = \chi_{\mathrm{lin}}(1 \mp \phi) = -\frac{N_{\mathrm{Na}}|\mu|^2}{2\epsilon_0 \hbar \Gamma_2}\left(\frac{\overline{\Delta}+i}{\overline{\Delta}^2+1}\right)(1 \mp \phi).$$

χ_{lin} denotes the linear susceptibility of the vapor, N_{Na} is the particle number density of the sodium atoms, and $\mu_{\mathrm{M}} = 1.72 \times 10^{-29}$ C m is the dipole matrix element of the transition. $\overline{\Delta} = 2\pi\Delta/\Gamma_2$ is the detuning $\Delta = \nu_{\mathrm{laser}} - \nu_{\mathrm{D_1}}$ of the laser beam with respect to the sodium-D_1 line normalized to the transverse relaxation rate Γ_2, i.e., the relaxation rate of the dipole moment of the transition. The linear absorption coefficient of the vapor is given by $2\alpha_0 := -k_0 \mathrm{Im}(\chi_{lin})$.

Under the given experimental conditions, the sodium-D_1 line can be modeled as a homogeneously broadened $J = \frac{1}{2} \rightarrow J' = \frac{1}{2}$-transition with a negligible population of the excited state [29]. In this case, the equation of motion for the longitudinally averaged orientation is given by [27]

$$\frac{\partial \phi}{\partial t} = -\gamma\phi + D\Delta_{\perp}\phi + \frac{1}{2\alpha_0 L}\{[P_{+,f}(0) - P_{+,f}(L)] - [P_{-,b}(L) - P_{-,b}(0)]\}. \quad (1)$$

The pump rates $P_{\pm,f/b}(0,L)$ of the forward and backward propagating beams are calculated at the entrance ($z=0$) and the exit ($z=L$) of the medium from the corresponding components of the electric field amplitudes:

$$P_{\pm} = \frac{3}{16}\frac{|\mu|^2}{4\Gamma_2 \hbar^2(\overline{\Delta}^2+1)}|E_{\pm}|^2. \quad (2)$$

The amplitudes of the electrical fields are connected by the transmission through the medium,

$$E_{+,f}(L) = \exp[-\alpha_0 L(1 - i\overline{\Delta})(1-\phi)]E_{+,f}(0), \quad (3)$$

$$E_{-,b}(0) = \exp[-\alpha_0 L(1 - i\overline{\Delta})(1+\phi)]E_{-,b}(L), \quad (4)$$

and by the free-space propagation

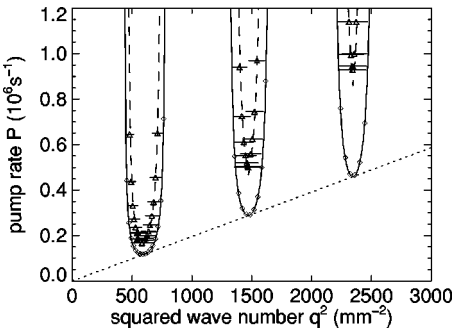

FIG. 4. Solid line represents linear stability analysis, diamonds plane wave simulations, triangles Gaussian beam simulations (pump rate given in the beam center), horizontal lines $1/\sqrt{e}$ radius of the Fourier mode, dashed line analytical approximation for Gaussian beam, see discussion below, and the dotted line connects the origin with the minimum of the first instability region of the linear stability analysis (see text). Parameters: $\gamma = 1.5\ \mathrm{s}^{-1}$, $\Gamma_2 = 10.45 \times 10^9\ \mathrm{s}^{-1}$, $\overline{\Delta} = 3.248$, $D = 232.27\ \mathrm{mm}^2\ \mathrm{s}^{-1}$, $N = 2.3 \times 10^{19}\ \mathrm{m}^{-3}$, $L = 15$ mm, $d = 77$ mm, and $R = 99\%$.

$$E_{\pm,b}(L) = R\exp\left(-\frac{id}{k_0}\Delta_{\perp}\right)E_{\mp,f}(L). \quad (5)$$

In addition, Eq. (5) takes into account the exchange of the polarization components by the quarter-wave plate and the losses due to reflection.

B. Linear stability analysis

The stationary homogeneous solution of Eqs. (1)–(5) is given by an implicit formula for the orientation, which is solved numerically:

$$2\alpha_0 L\gamma\phi_0 = P_0[1 - e^{-2\alpha_0 L(1-\phi_0)} - Re^{-2\alpha_0 L(1-\phi_0)} \times (1 - e^{-2\alpha_0 L(1+\phi_0)}]. \quad (6)$$

The stability of the solution of Eq. (6) against perturbations of the form $\delta\phi \sim e^{\mu t + i\vec{q}\cdot\vec{r}_{\perp}}$ is determined by the growth exponent μ of the perturbation, which is

$$\mu = -\gamma - Dq^2 - P_0 e^{-2\alpha_0 L(1-\phi_0)}(1 + Re^{-2\alpha_0 L(1+\phi_0)}) - RP_0 e^{-2\alpha_0 L(1-\phi_0)}(1 - e^{-2\alpha_0 L(1+\phi_0)})\left[\cos\left(\frac{dq^2}{k_0}\right) + \overline{\Delta}\sin\left(\frac{dq^2}{k_0}\right)\right].$$

The curve of marginal stability, which is given by $\mu = 0$, is depicted as a solid line in Fig. 4. Below the curve the linear growth exponent is negative, the homogeneous steady state is stable. Above the curve it is unstable.

The result of the linear stability analysis predicts the existence of multiple instability regions. This is expected for single-mirror feedback experiments because of the spatial periodicity of the Talbot effect [25,30,31]. The experimentally observed boundaries of the instability regions show a good qualitative agreement with the marginal stability curve.

Both show an increased damping of the higher-order instabilities, which results from diffusion [25,32].

The threshold pump power for a beam with a radius of 1.37 mm and the critical threshold pump rate as determined from the LSA (Fig. 4) amounts to 44 mW, 109 mW, and 174 mW for the three instability regions. This is of the same order of magnitude as the experimental values (28 mW, 79 mW, and 140 mW, see Fig. 3). Also, the experimentally observed wave numbers show a reasonable good agreement with the LSA (see Figs. 4 and 3). A complete agreement of the absolute values cannot be expected, since the conversion of experimental values to model parameters underlies some uncertainties. For example, the change of the pumping efficiency due to hyperfine splitting is only accounted for by a constant factor (3/16 in Eq. (2), Ref. [33]). Some deviations in the wave numbers are expected due to uncertainties in the determination of the effective mirror distance resulting from the insertion of the Fourier filter.

However, the ratios of the measured critical wave numbers are in good agreement with the prediction of the linear stability analysis. In contrast, the relative thresholds of the instabilities do not match the expectation from the linear stability analysis: The ratio of the threshold of the second region to the one of the first is 2.8 in the experiment, whereas it is 2.5 in the LSA. The corresponding numbers for the third region are 5.0 (experiment) and 3.9 (LSA). These figures indicate that there is some additional damping for higher wave numbers. This fact is also illustrated by the lines added to the Figs. 4 and 3: Whereas in the data obtained from the LSA a straight line connecting the origin with the minimum of the first region intersects the two other minima with a high precision (Fig. 4), this is clearly not the case in the experiment (Fig. 3).

C. Numerical results

One questionable assumption made in the analysis is the one of a homogeneous profile of the laser beam. While a plane wave input is assumed in the linear stability analysis, the experiment is performed with a Gaussian beam. For a more detailed analysis, numerical simulations were performed with a Gaussian input beam and a plane wave.

By means of Fourier filtering a stripe pattern with a certain wave number was selected analogous to the experiments. The threshold was determined by a step-by-step increase of the pump rate with a resolution of $\leqslant 1\%$ of the threshold value. The results of the simulations are shown in Fig. 4. As expected, the simulations with a plane wave input reproduce the predictions of the linear analysis within the used precision. For a Gaussian input beam, as it is used in the experiment, the threshold for pattern formation is significantly higher. This observation is often explained by the intuitive assumption that a region with an extent of at least some wavelengths of the pattern has to be above threshold for the development of a structure. In this case, the deviation should be less pronounced for the higher-order instability regions, since the aspect ratio increases with increasing wave number. Obviously, the contrary is true. Therefore, a more refined model has to be considered.

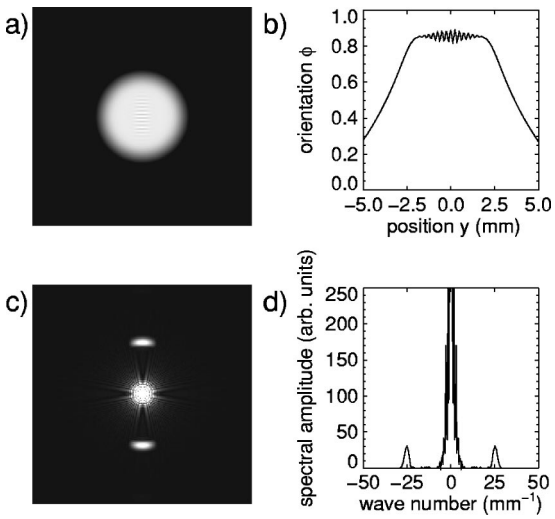

FIG. 5. Typical distribution of orientation slightly above threshold from numerical simulation. (a) orientation, (b) vertical cut, (c) numerically calculated Fourier transform, and (d) vertical cut through Fourier transform.

D. Influence of finite size effects

A typical distribution of the orientation ϕ obtained in a numerical simulation with a Gaussian beam slightly above threshold is shown in Fig. 5. Stripe patterns occur in a certain region in the center of the beam. Their wavelengths are small compared to the extent of the nearly homogeneous plateau present in the beam center (between about $y=-2.5$ mm and $y=2.5$ mm). This observation suggests a two-scale ansatz for the orientation distribution of the patterned state:

$$\Phi(x)=\Phi_h(x)+A\exp\left(-\frac{x^2}{2w_\Phi^2}\right)\cos(q_0x). \tag{7}$$

The spatial scale $1/q_0$ of the pattern is separated from the scale of the quasihomogeneous background $\Phi_h(x)$ that is given by the orientation profile below threshold. The assumption of a Gaussian envelope for the amplitude of the pattern in real space is based on the observation that the Fourier components [cf. Fig. 5(d)] have a profile, which can be very well approximated by a Gaussian distribution. The analysis of the results of the numerical simulations indicate that the width w_Φ of the pattern is approximately given by the size Δx of the area that is above threshold. Therefore, an upper bound of the size of the pattern is then given by

$$w_\Phi \lesssim \Delta x=\left[-\frac{w_0^2}{2}\ln\left(\frac{P_c}{P_0}\right)\right]^{1/2}. \tag{8}$$

w_0 denotes the $1/e^2$ radius of the Gaussian pump profile. The pump rate at the center of the beam is given by P_0, while P_c denotes the critical pump rate for the wave number q from the linear analysis. Inequality (8) is equivalent to a lower bound for w_q, the $1/\sqrt{e}$ radius of the pattern's Fourier component

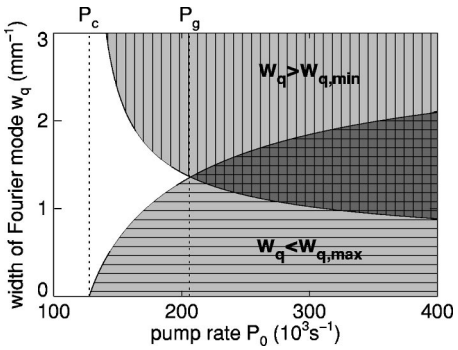

FIG. 6. Determination of the threshold in Gaussian beams. Explanations are given in text.

$$w_q(P_0) \gtrsim w_{q,min}(P_0) = \frac{1}{w_\Phi}. \tag{9}$$

The area corresponding to inequality (9) is hatched vertically in Fig. 6.

The estimate given is a lower bound for the size of a Fourier component. A mechanism providing an upper bound can be derived from the numerical results presented in Fig. 4. The small horizontal lines at each triangle (representing the data points stemming from simulations with a Gaussian input beam) denote the $1/\sqrt{e}$ radii w_q of the Fourier modes of the stripe patterns. In the minima of the instability regions, the size of the Fourier components agrees with the width of the curve of marginal stability at the respective pump rate. Beyond threshold, it is found that the lines representing the numerically calculated $1/\sqrt{e}$ radii of the Fourier components extend till the ''closest'' border of the instability regions that are obtained from the linear analysis of the homogeneous state. As a conclusion, the maximum width of a Fourier mode is limited by the curve of marginal stability. Hence, an upper estimate for the width of the Fourier peaks is given by

$$w_q(P_0) \lesssim w_{q,max}(P_0) = \min\{|q_0 - q_L(P_0)|, |q_0 - q_R(P_0)|\}. \tag{10}$$

q_L and q_R denote the left and right borders of the curve of marginal stability at a given pump rate P_0. The area corresponding to condition (10) is hatched horizontally in Fig. 6.

The lowest pump rate P_0, where both criteria [Eqs. (9) and (10)], are fulfilled, is the intersection point of the curves $w_{q,max}(P_0)$ and $w_{q,min}(P_0)$. It determines the threshold pump rate in a Gaussian beam and the size of the Fourier mode, and hence the size of the pattern. The results of the calculation are plotted in Fig. 4 as a dashed line for each instability region. The curves agree surprisingly well with the results obtained from the simulations with a Gaussian beam input. Also the agreement with the experimentally determined instability regions is improved. The ratios between the thresholds of the different instability regions ($P_2/P_1 = 3.0$ and $P_3/P_1 = 5.5$) are considerable closer to the values given in the experiment than the result of the usual linear stability analysis. We conclude that the procedure described above is a suitable extension of the conventional linear stability analysis of the homogeneous state for the case of a Gaussian input beam.

Compared with some other previous results [34,35] the influence of the Gaussian beam is relatively weak in the system under study. Essentially, it results in an increase of the threshold of pattern formation. However, in the case of saturable media, for which the instability regions possess an upper bound (cf., e.g., Ref. [32]), the presented effect may result in the suppression of the pattern formation.

IV. OUTLOOK

The presented experimental method is a powerful tool to determine the linear stability properties of the unstructured state. It is of interest to apply the method to systems for which a linear stability analysis is not possible, because either there is no reliable model available or the complexity of a model prevents analysis. In such a case, the experimentally obtained marginal stability curves provide a first insight into the relevant length scales and possible competition between different instabilities. This might already give some insight in the pattern selection process, since often some arguments can be already based on the linear stability properties (cf. many of the papers cited in the Introduction).

ACKNOWLEDGMENT

This work was supported by the Deutsche Forschungsgemeinschaft.

[1] M.C. Cross and P.C. Hohenberg, Rev. Mod. Phys. **65**, 851 (1993).
[2] D. Walgraef, *Spatio-Temporal Pattern Formation: With Examples from Physics, Chemistry, and Materials Science* (Springer-Verlag, New York 1996).
[3] S. Residori, P.L. Ramazza, E. Pampaloni, S. Boccaletti, and F.T. Arecchi, Phys. Rev. Lett. **76**, 1063 (1996).
[4] T. Ackemann, Y.A. Logvin, A. Heuer, and W. Lange, Phys. Rev. Lett. **75**, 3450 (1995).
[5] Y.A. Logvin, T. Ackemann, and W. Lange, Phys. Rev. A **55**, 4538 (1997).
[6] Z.H. Musslimani and L.M. Pismen, Phys. Rev. A **59**, 1571 (1999).
[7] M.A. Vorontsov and A.Y. Karpov, J. Opt. Soc. Am. B **14**, 34 (1997).
[8] M.L. Berre, D. Leduc, E. Ressayre, and A. Tallet, Asian J. Phys. **7**, 483 (1998).
[9] H. Levine, W.J. Rappel, and H. Riecke, Phys. Rev. A **43**, 1122 (1991).
[10] I. Mutabazi and C.D. Andereck, Phys. Rev. Lett. **70**, 1429 (1993).
[11] W.S. Edwards and S. Fauve, Phys. Rev. E **47**, R788 (1993).
[12] A. Kudrolli, B. Pier, and J.P. Gollub, Physica D **123**, 99 (1998).
[13] C. Wagner, H.W. Müller, and K. Knorr, Phys. Rev. Lett. **83**, 308 (1999).

[14] C. Wagner, H.W. Müller, and K. Knorr, Phys. Rev. E **62**, R33 (2000).
[15] M. Silber, C.M. Topaz, and A.C. Skeldon, Physica D **143**, 205 (2000).
[16] F.H. Busse, Rep. Prog. Phys. **41**, 1929 (1978).
[17] M.A. Dominguez-Lerma, D.S. Cannell, and G. Ahlers, Phys. Rev. A **34**, 4956 (1986).
[18] D.B. White, J. Fluid Mech. **191**, 247 (1988).
[19] E.V. Degtiarev and M.A. Vorontsov, J. Opt. Soc. Am. B **12**, 1238 (1995).
[20] R. Martin, A.J. Scroggie, G.-L. Oppo, and W.J. Firth, Phys. Rev. Lett. **77**, 4007 (1996).
[21] S.J. Jensen, M. Schwab, and C. Denz, Phys. Rev. Lett. **81**, 1614 (1998).
[22] A.V. Mamaev and M. Saffman, Phys. Rev. Lett. **80**, 3499 (1998).
[23] T. Ackemann, B. Giese, B. Schäpers, and W. Lange, J. Opt. B: Quantum Semiclassical Opt. **1**, 70 (1999).
[24] R. Neubecker and E. Benkler, Phys. Rev. E **65**, 066206 (2002).
[25] W.J. Firth, J. Mod. Opt. **37**, 151 (1990).
[26] G. D'Alessandro and W.J. Firth, Phys. Rev. Lett. **66**, 2597 (1991).
[27] A. Aumann, T. Ackemann, E. Große Westhoff, and W. Lange, Phys. Rev. E **66**, 046220 (2002).
[28] M.L. Berre, D. Leduc, E. Ressayre, A. Tallet, and A. Maître, Opt. Commun. **118**, 447 (1995).
[29] W. Lange, T. Ackemann, A. Aumann, E. Büthe, and Y.A. Logvin, Chaos, Solitons Fractals **10**, 617 (1999).
[30] E. Santamato, E. Ciaramella, and M. Tamburrini, Mol. Cryst. Liq. Cryst. Sci. Technol., Sect. A **251**, 127 (1994).
[31] T. Ackemann and W. Lange, Appl. Phys. B: Lasers Opt. **72**, 21 (2001).
[32] T. Ackemann, A. Aumann, E. Große Westhoff, Y.A. Logvin, and W. Lange, J. Opt. B: Quantum Semiclassical Opt. **3**, S124 (2001).
[33] M. Möller and W. Lange, Phys. Rev. A **49**, 4161 (1994).
[34] M.N. Ouarzazi, P.A. Bois, and M. Taki, Phys. Rev. A **53**, 4408 (1996).
[35] E. Louvergneaux, Phys. Rev. Lett. **87**, 244501 (2001).